Journal of Atmospheric and Solar–Terrestrial Physics 211 (2020) 105449

Contents lists available at ScienceDirect

Journal of Atmospheric and Solar-Terrestrial Physics

journal homepage: www.elsevier.com/locate/jastp

Climatology of polar ionospheric density profile in comparison with mid-latitude ionosphere from long-term observations of incoherent scatter radars: A review

Eunsol Kim [a,b], Geonhwa Jee [b,c,*], Eun-Young Ji [d], Yong Ha Kim [a], Changsup Lee [b], Young-Sil Kwak [e,f], Ja-Soon Shim [g]

[a] Chungnam National University, Daejeon, Republic of Korea
[b] Korea Polar Research Institute, Incheon, Republic of Korea
[c] Department of Polar Science, Korea University of Science and Technology, Daejeon, Republic of Korea
[d] School of Space Research, Kyung Hee University, Yongin, Republic of Korea
[e] Korea Astronomy and Space Science Institute, Daejeon, Republic of Korea
[f] Department of Astronomy and Space Science, Korea University of Science and Technology, Daejeon, Republic of Korea
[g] The Catholic University of America, NASA GSFC, Greenbelt, MD, USA

ARTICLE INFO

Keywords:
Polar ionosphere
Climatology
Incoherent scatter radar
Review

ABSTRACT

Although the horizontal density structures of the polar ionosphere have been extensively studied mostly using the F-region peak density or total electron content, there are relatively few studies on the vertical density structures. In this review, we present the climatology of the polar ionospheric density not only in the F-region but also in the E-region and topside ionosphere, in comparison with the mid-latitude ionosphere, using long-term incoherent scatter radar (ISR) observations at Millstone Hill, Tromsø, and Svalbard. The ISR data during the period of 1995–2015 are analyzed to study on the variations with local time, season, and solar/geomagnetic activity. The diurnal variations of the F-region density are much smaller in the polar region than in the mid-latitude, particularly in summer. At Svalbard, there is a characteristic double-peak structure in the diurnal variation of the polar ionosphere in winter only for high solar activity. The diurnal variation of hmF2 decreases with increasing latitude and eventually disappears at Svalbard for low solar activity but the hmF2 and its diurnal variations in the polar ionosphere are remarkably enhanced for high solar activity. The distinctive irregularity in the mid-latitude F1-layer nearly disappears in the polar region, especially at Svalbard. The anomalous seasonal variations of the F-region density are less evident in the polar ionosphere especially for low solar activity and for high magnetic activity conditions. The polar E-region density shows characteristic nighttime peaks induced by auroral precipitation but it does not necessarily increase with solar activity. The topside ionospheric density variations are much stronger in the polar region for high solar activity. Finally, it is found that the polar ionospheric density profiles more strongly respond to increasing solar activity as well as the magnetic activity compared with the mid-latitude ionosphere.

1. Introduction

The ionospheric density is chiefly produced by solar extreme ultraviolet (EUV) radiation, depleted by recombination with atmospheric molecules and redistributed by electric field and/or neutral winds. In addition to these processes, the polar ionosphere including the auroral oval and polar cap/cusp is characterized by the coupling with the magnetosphere along the geomagnetic field lines, which results in unique characteristics of the polar ionosphere such as strong plasma convection, energetic particle precipitations, and joule/frictional heating. The auroral oval is the luminous boundary between the open geomagnetic field lines, which connect out to the solar wind, and the closed field lines. The auroral oval itself lies largely on the closed field lines. The polar cap, poleward of the auroral oval, is therefore a region of the open field lines, connecting out to the solar wind, generally far downstream of the Earth. The auroral energetic particles precipitate into

* Corresponding author. Korea Polar Research Institute, Incheon, Republic of Korea.
E-mail address: ghjee@kopri.re.kr (G. Jee).

https://doi.org/10.1016/j.jastp.2020.105449
Received 26 March 2020; Received in revised form 2 September 2020; Accepted 8 September 2020
Available online 28 September 2020

the upper atmosphere from the magnetosphere along the magnetic field lines, resulting in characteristic features such as auroral emissions, ion production, and heating mainly in the auroral oval. In the cusp region in which the magnetosheath plasma has a direct access to the ionosphere, there are additional productions in the E-region by energetic proton precipitation and in the F-region by soft electron precipitation. In the polar cap within the auroral oval and the cusp there exist a homogeneous electron precipitation (i.e., a polar rain), which originates with the suprathermal component of the solar wind electron population, and sun-aligned arcs, which are intense auroral emissions imbedded in the polar rain. As for the transport processes affecting the ionospheric density distribution in the polar region, the anti-sunward plasma convection carries the plasma from the dayside at lower latitudes to the nightside across the polar cap, which produces characteristic plasma density structures such as tongue of ionization (TOI) and polar cap patch. Compared with the low and mid-latitude ionosphere, however, the polar ionospheric density structure has not been well established, presumably due to the relatively limited observations from ground or space. In previous studies, moreover, much attention has been paid to the horizontal structures of the ionospheric density such as polar cap patch, TOI, ionization trough, ionization hole and auroral blobs, mostly using the measurements of the F-region peak density (NmF2) or total electron content (TEC). However, there are relatively few studies on the characteristic features of the vertical density structures including the E-region and topside ionosphere.

The variations of the F-region density profile in the polar ionosphere have mainly been investigated by using incoherent scatter radar (ISR) and/or ionosonde observations (e.g., Fontaine, 2002; Zhang et al., 2005; Cai et al., 2007; Moen et al., 2008; Ratovsky et al., 2014; Xu et al., 2014). Using the European Incoherent Scatter (EISCAT) radar observations at Tromsø and Svalbard, Cai et al. (2007) performed a statistical investigation of the seasonal variations of the polar ionospheric density. Their results showed that the winter anomaly appears only at Tromsø during solar maximum but it does not appear at Svalbard. It was also found that the polar ionosphere shows a weak diurnal variation in summer due to the extended period of solar production, but in winter two peaks appear near the magnetic local noon and pre-midnight at Svalbard. They suggested that the first peak is caused by soft particle precipitation from the cusp and the second peak seems likely to be transport effects related to substorms. Fontaine (2002) reported brief observational results obtained from the EISCAT radars, showing the E-region nighttime density enhancement in the auroral region and the effect of particle precipitation on the dayside ionosphere in the cusp region in winter. Moen et al. (2008) studied on the diurnal variations of the F2-region plasma density using the data from EISCAT Svalbard radar (ESR) and showed that the NmF2 exhibits one maximum at around 12 MLT and another at around 23 MLT, which was explained by the cross-polar cap transport of solar EUV ionized plasma from dayside to nightside. Xu et al. (2014) investigated the climatological features of NmF2 including diurnal and seasonal variations in the northern and southern polar regions using the long-term observations from ISR at Svalbard, dynasonde at Tromsø and digisonde at Zhongshan Antarctic station. They found that the maximum NmF2 occurs at local noon in the auroral region (i.e., Tromsø) but at magnetic local noon in the cusp region (i.e., Svalbard and Zhongshan station), due to the productions by solar EUV and soft particle precipitation, respectively. In addition to the noontime peak, they also found the second peak at pre-midnight sector at Svalbard in winter during solar maximum condition, which was explained to be caused by plasma transport from dayside. Regarding the seasonal variations, it was found that the semiannual anomaly always occurs in both the auroral and polar cap regions during solar maximum condition. Using the empirical models based on long-term ISR observations in the middle and high latitudes, Zhang et al. (2005) reported seasonal variations such as annual and semiannual anomalies showing clear latitude, longitude, and altitude dependencies.

Most of these previous studies on the polar ionosphere have been focused on the F-region peak density. However, the polar ionosphere is known to show unique features not only in the F-region peak density but also in the whole profile of plasma density including the E-region and the topside ionosphere. In particular, the E-region density is characterized by additional production due to the energetic particle precipitations (Baron, 1974; Hunsucker, 1975) and the topside ionospheric density is closely coupled to the magnetosphere by the ion outflows in the polar region. These processes should produce unique density structures in the polar E-region and topside ionosphere. In this review, we comprehensively investigate the general characteristics of the entire density profiles in the auroral and polar cap regions in comparison with the mid-latitude ionosphere, using long-term ISR observations from Tromsø, Svalbard and Millstone Hill, for various geophysical conditions, in order to emphasize the distinguished features of the polar ionospheric density profiles bringing new insight into the polar region. In the following sections, a brief introduction for ISR observations used for this study will be described with the analysis of the data and then the results and discussions will be followed.

2. Incoherent scatter radar observations

The electron density profiles have been observed by ground-based radar instruments such as ISR and ionosonde. Although the ionosonde observations have been much more extensively performed over the whole globe, it is mostly concentrated in the low and mid-latitude ionosphere and there are only a few observations in the high-latitude region particularly in the southern hemisphere. In the northern polar region, the EISCAT Scientific association has been operating ISR systems over the northern Scandinavian countries since the first radar (Tromsø UHF) has started its observation in 1981 and greatly contributed to the upper atmospheric researches (Rishbeth and Van Eyken, 1993). We use the long-term data of electron density profiles measured by the EISCAT radars at Tromsø (EISCAT) and Svalbard (ESR) for the polar ionosphere and also Millstone Hill ISR as a representative mid-latitude ionosphere to be compared with the polar ionosphere during the period of 1995–2015. Table 1 shows the information of each station and the observation periods for this study.

The physical properties of the ionosphere in the auroral oval, polar cap, and polar cusp are very different from each other and therefore it is critical to consider the locations of the observation sites with respect to these polar regions in order to properly interpret the results of the data analysis. Fig. 1 shows the approximate locations of the ISR stations relative to the auroral oval in the northern hemisphere. The boundaries of the auroral oval in this figure are adopted from Xiong et al. (2014) which statistically determined the boundaries using 10-year magnetic field data measured by the Challenging Minisatellite Payload (CHAMP) satellite. The boundaries vary with magnetic activity as expected but show no dependence on solar EUV flux or season. Note that the poleward boundary of the auroral oval near the magnetic local midnight does not vary with Kp level. In this figure, the EISCAT radar at Tromsø is located near the equatorward boundary of the auroral oval during nighttime but in the subauroral region during daytime for geomagnetically quiet condition ($Kp < 2$). As the magnetic activity increases, the EISCAT is mostly located in the auroral oval except for around the magnetic local noon. The ESR at Svalbard is located in the auroral oval during daytime but at night it is mostly located in the polar cap. Since the poleward boundary of the auroral oval does not change with magnetic activity

Table 1
Location of three incoherent scatter radar stations and period of observations used in the present study.

	Latitude	Longitude	Magnetic Lat.	Obs. period
Millstone Hill	42.62°N	288.51°E	53°N	1999–2013
Tromsø (EISCAT)	69.35°N	19.14°E	66°N	1995–2015
Svalbard (ESR)	78.09°N	16.01°E	75°N	1999–2015

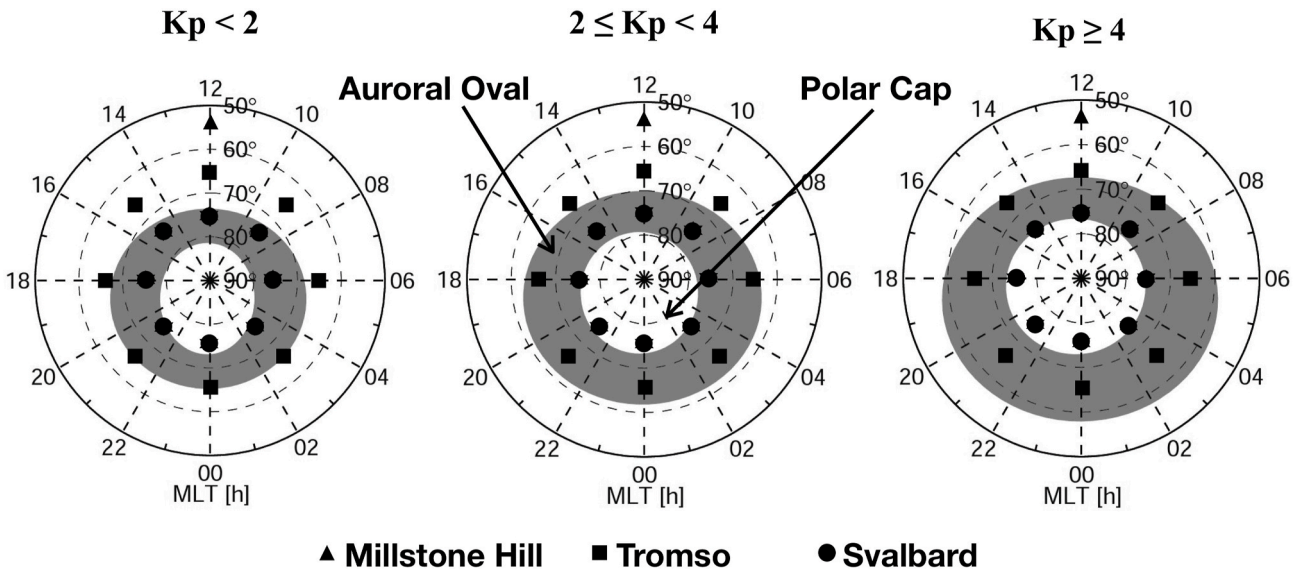

Fig. 1. Schematic illustration of the locations of three incoherent scatter radar stations for different geomagnetic conditions (adopted from Xiong et al., 2014).

near the magnetic midnight, the nighttime ESR is considered to be always located in the polar cap regardless of the magnetic activity level. Note that the ESR is mostly located near the cusp at around magnetic local noon. These relative locations of EISCAT and ESR should be kept in mind throughout the discussions of the results of the study.

The observation period for this study includes the solar cycle 23 and 24, as can be seen in Fig. 2 that shows, at the top two panels, the daily F10.7 and Kp indices obtained from NASA/OMNI website (http://omniweb.gsfc.nasa.gov/form/dx1.html). The red lines at F10.7 = 120 and Kp = 2 represent the criteria for low/high solar activity and quiet/disturbed geomagnetic activity conditions, respectively. The ISR data were obtained from the EISCAT UHF radar at Tromsø and the ESR radar with a 42-m antenna at Svalbard, which were downloaded from NIPR database (pc115.seg20.nipr.ac.jp/www/eiscatdata/ne_te_ti_vi.html), and the Millstone Hill ISR radar, which was obtained from the Madrigal CEDAR database (http://cedar.openmadriga.org). We used all available data from these radars in the observation period with 1-min integration time. The lower three panels in Fig. 2 show the data coverage of the three ISR observations and the white sections indicate the time of the day at which the data are available.

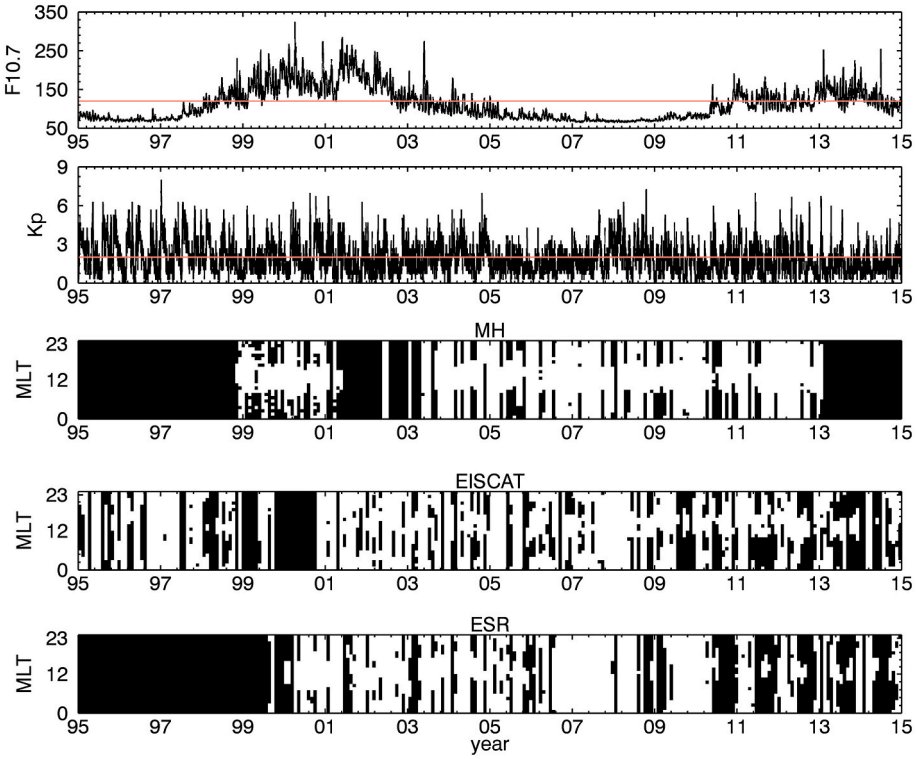

Fig. 2. The daily F10.7 and mean Kp indices during the period of 1995–2015 at the top panels. The red lines represent criteria to divide low/high solar activity and quiet/disturbed geomagnetic activity conditions. The bottom three panels show the data coverages at each hour-month grids in the MLT vs. year coordinate for Millstone Hill (MH), Tromsø (EISCAT) and Svalbard (ESR) stations.

For the analysis of the data, a vertical interpolation with a 5-km altitude step was applied to each measured electron density profiles at which the number of data points is greater than 10 within the observed altitude range, and then the hourly-mean density profiles are reproduced for the analysis. The resulting density profiles are sorted by low and high solar/geomagnetic activity levels (F10.7 < 120, F10.7 > 120; Kp < 2, Kp > 2) for equinox (3, 4, 9, 10), summer (5, 6, 7, 8), and winter (11, 12, 1, 2) solstices. With these geophysical data bins, the

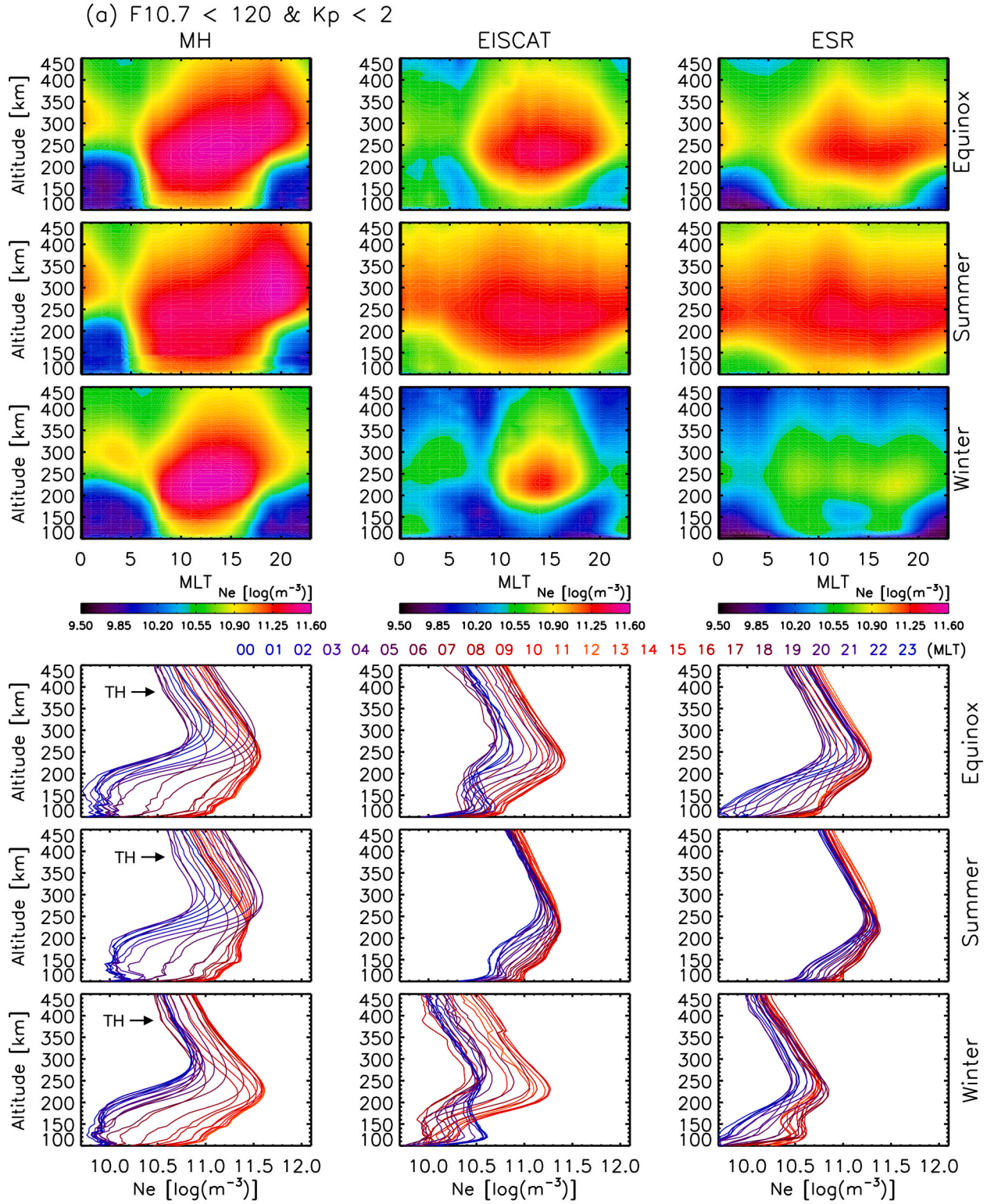

Fig. 3. a. Hourly mean electron density profiles with magnetic local time during equinox, summer and winter for low solar (F10.7 < 120) and low geomagnetic (Kp < 2) activities at Millstone Hill (MH; left), Tromsø (EISCAT; middle), and Svalbard (ESR; right) stations. The diurnal variations of the density profiles are presented in the contour (top) and line plots (bottom). 'TH' in the line plots indicates the transition height between O^+ and H^+ ion dominated regions during nighttime. **b**. Same as Fig. 3a but for low solar (F10.7 < 120) and high geomagnetic (Kp > 2) activity conditions. **c**. Same as Fig. 3a but for high solar (F10.7 > 120) and low geomagnetic (Kp < 2) activity conditions. **d**. Same as Fig. 3a but for high solar (F10.7 > 120) and high geomagnetic (Kp > 2) activity conditions.

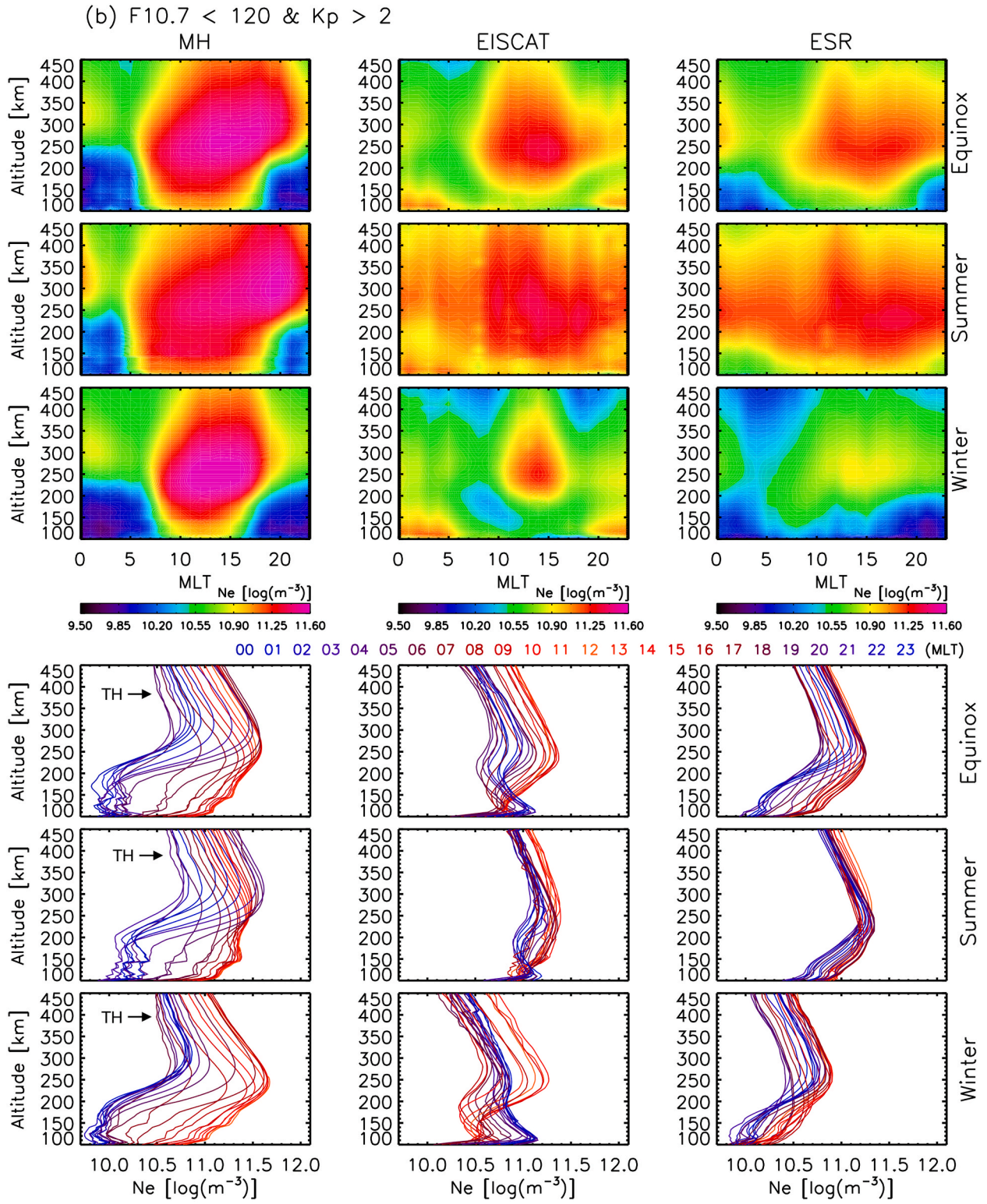

Fig. 3. (*continued*).

ionospheric parameters are determined from the reproduced hourly-mean density profiles, including the F2-layer peak density (NmF2) and height (hmF2), the E-region peak density (NmE), and the ionospheric slab thickness (IST) and scale height (ISH). The NmF2 was determined as a maximum density in the altitude range of 200–450 km with the corresponding peak altitude as hmF2 in order to avoid the E-region density that can be even larger than F-region density in the polar region. The NmE was determined at the altitude where the gradient of the density profiles changes from positive to negative with increasing altitude or where the density gradient becomes smaller below 140 km. The determination of IST and ISH will be described in the section for the topside ionosphere.

In the procedure of data analysis, the limitations of the ISR observations are considered. For example, the data below about 80 km

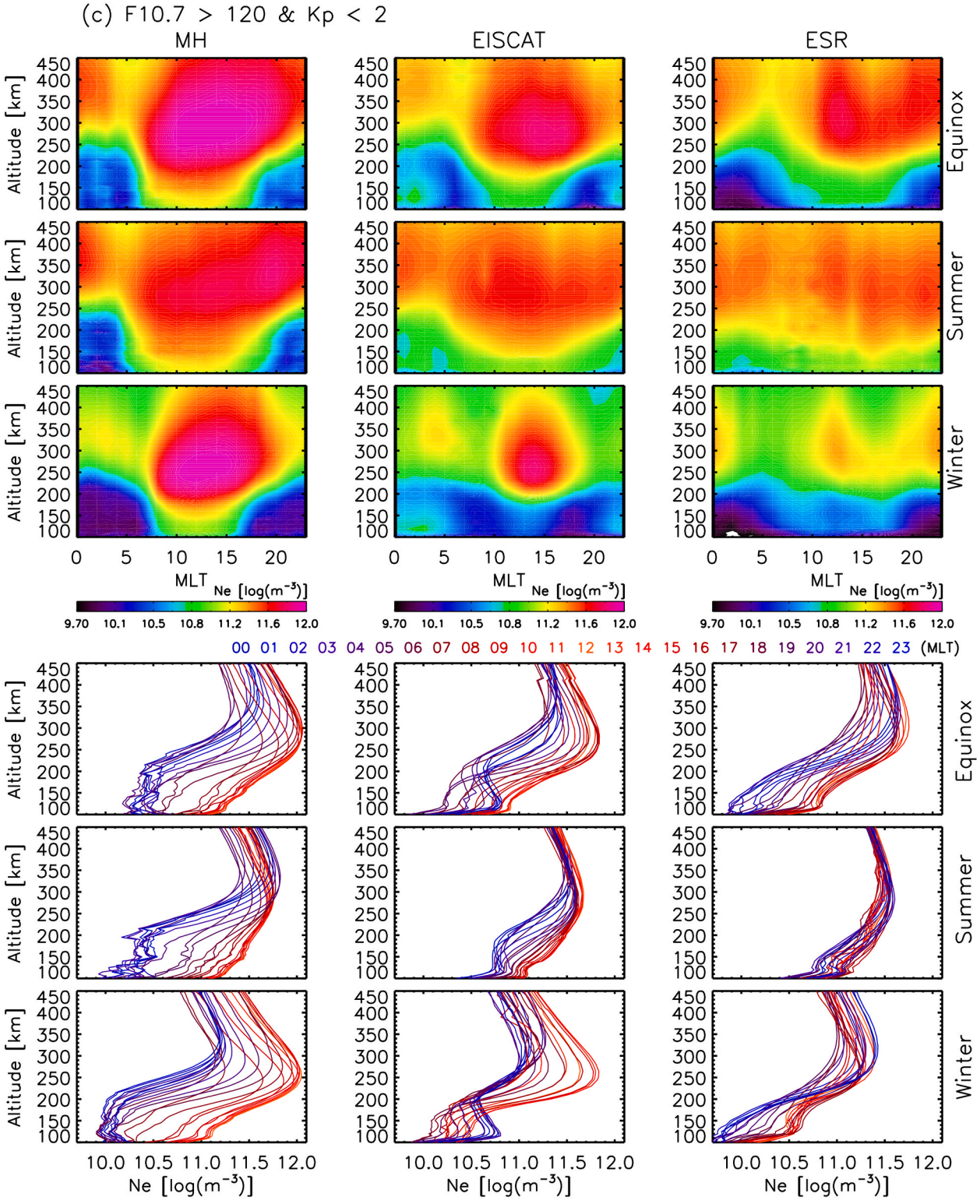

Fig. 3. (*continued*).

altitude were excluded due to the large uncertainty that is known to be caused by atmospheric scatter or instrumental effects (Ranta et al., 1985; Hargreaves et al., 1987). The uncertainty of the ISR measurements also tends to increase at higher altitude where the signal-to-noise ratio becomes very low as the electron density decreases (Caton et al., 1996). With these limitations of the ISR observations at low and high altitude regions, the density profiles only from 100 to 450 km altitude are utilized for this study. Regarding the general estimation errors of the ISR, Vallinkoski and Lehtinen (1990) discussed the effect of a priori knowledge of a parameter on the estimation accuracy of other parameters in the incoherent scatter radar observation.

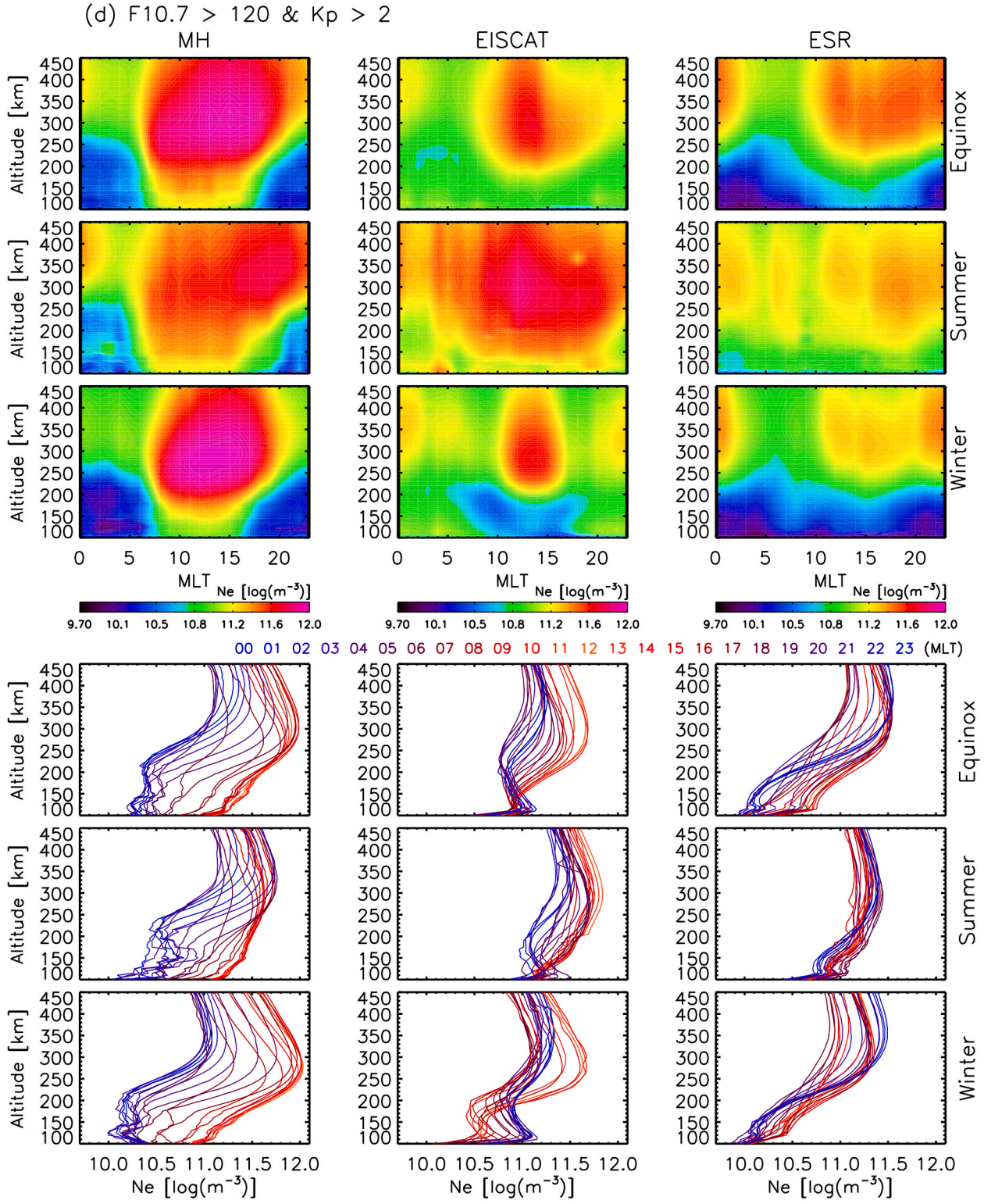

Fig. 3. (*continued*).

3. Results and discussions

3.1. F-region in the polar ionosphere

3.1.1. Diurnal variations of the F-region density

Fig. 3a-d shows the hourly mean electron density profiles with magnetic local time (MLT) as contour and line plots at Millstone Hill (MH), Tromsø (EISCAT), and Svalbard (ESR) for equinox, summer, and winter during low and high solar/magnetic activities. The ionospheric density varies principally with solar EUV production which solely depends on the solar zenith angle varying with local time, latitude and season, in addition to the solar activity. Therefore, the overall ionospheric density is supposed to be smaller in the polar region than in the mid-latitude region, due to the reduced solar EUV production by

increased solar zenith angle. The diurnal variations should also be significantly different from the mid-latitude ionosphere especially in solstice when a complete dark or sunlit condition exists in the polar region. However, the observations show much greater variabilities of the polar ionosphere than expected, probably due to characteristic ion productions and strong transport processes induced by magnetospheric energy inputs, as well as different seasonal characteristics of solar illumination in the region.

The most noticeable characteristics of the polar ionosphere in Fig. 3 is that the diurnal variations of the density profiles are in general greatly reduced as expected. In particular, it nearly disappears in the topside ionosphere at both Tromsø and Svalbard in summer when the upper atmosphere is always sunlit (see line plots of the density profiles at the lower panels of Fig. 3). In winter, on the other hand, the solar production almost disappears and other factors such as particle precipitation and plasma transport become more important to produce different diurnal variations. Especially at Svalbard for high solar activity (Fig. 3c), there are two density peaks at around 12 MLT and 23 MLT. This double-peak structure is most obvious in winter but does not exist in summer. In equinox, the nighttime density peak is not conspicuous as in winter but broadly distributed at around 20 MLT. During disturbed condition, the double-peak structure becomes less evident even in winter as shown in Fig. 3d. Although there is a noticeable density enhancement at around magnetic local midnight in winter, the daytime density does not show any noticeable peak. The double-peak structure has been reported at a few previous studies also using ESR observations (Cai et al., 2007; Moen et al., 2008; Xu et al., 2014). Cai et al. (2007) found that the density reaches a maximum at around 23 MLT with a smaller secondary peak at around 12 MLT in winter during solar maximum period of 1999–2003. Moen et al. (2008) also found the similar double-peak structure in the diurnal variations of NmF2 at Svalbard in Feb. 2001 and Oct. 2002 during solar maximum condition. Xu et al. (2014) reported the double-peak structure at Svalbard (Longyearbyen) for both solar minimum and maximum conditions but with different local times. The peaks at solar minimum appear at 08 MLT and 19 MLT with a daily minimum near the magnetic local noon while the peaks at solar maximum appear at the same magnetic local times as in the current study (i.e., at around magnetic local noon and pre-midnight sector). However, the double-peak structure for low solar activity was not found in Fig. 3a and b, which implies that the double-peak structure at Svalbard may be a characteristic feature occurring only for high solar activity condition.

When the ESR observation is performed at the cusp near magnetic local noon for geomagnetically quiet condition ($Kp < 2$), the soft particle precipitation induces ionization to form the daytime peak. Note that the daytime peak is less clear for $Kp > 2$ probably because the location of ESR is off the cusp region due to the expansion of the auroral oval to lower latitude as Kp increases (see Fig. 1). More detailed discussions of the soft particle effects on the daytime peak can be found at Cai el al. (2007). However, there is an alternative attempt to explain the daytime peak at magnetic local noon. Moen et al. (2008) attributed it to the solar EUV ionized plasma being transported into the cusp and subsequently to the midnight sector across the polar cap. Further investigation would be required to identify which factor is more important to produce the daytime peak in winter at Svalbard. As for the nighttime density peak, which seems to be more crucial for the formation of the double-peak structure, it appears at around the magnetic local midnight only for high solar activity. Cai et al. (2007) suggested a possible relation with substorm events. Moen et al. (2008) attempted to explain the nighttime peak caused by the solar wind controlled plasma transport from dayside to nightside across the polar cap, which is also responsible for the TOI and/or the polar cap patch. Even though the mean convection pattern is less dependent on the solar cycle compared to the dependence of the interplanetary magnetic field (IMF) condition, Forster and Haaland (2015) showed that the antisunward ion drift velocity increases with increasing solar activity. Dandekar (2002) also found that the occurrence and strength of polar cap patches increases with increasing solar activity. Besides, major geomagnetic storms accompanying energetic particle precipitation and strong plasma convection tend to more frequently occur near the peak of solar cycle (Gonzalez et al., 1990; Obridko et al., 2013; Le et al., 2013).

All these aspects of solar cycle dependency seem to support the double-peak structure occurring only for high solar activity.

3.1.2. F1-layer

In the mid-latitude ionosphere, the daytime F-region ionosphere splits into the F1- and F2-layers but when the solar EUV production ends at night the F1-layer begins to be abated and eventually disappears before the midnight due to the rapid recombination rate in the region. The daytime F1-layer appears at around 150 km altitude for all seasons but strongest in summer (see the line density profiles in Fig. 3). Note that the peak of the F1-layer generally appears at the similar height to the peak of the solar EUV production rate in the F-region. The F1-layer is less pronounced as the solar zenith angle increases: it becomes less distinctive in winter than in summer and at higher latitudes (Rishbeth and Garriott, 1969), which is consistent with the ISR observations. At Millstone Hill, the F1-layer is most distinctive in summer but least in winter as theory indicated. In the polar region, it is not as noticeable as in the mid-latitude region and almost disappears at Svalbard except for summer when the F1-layer appears only as a smooth bulge at around 150 km. Therefore, it is confirmed that as the solar zenith angle increases from low to high latitude, the splitting of the F-region ionosphere into the F1- and F2-layers becomes less pronounced and the F1-layer eventually disappears in the polar winter ionosphere. With regard to solar activity dependence of the F1-layer, it is found that the mid-latitude F1-layer is less distinctive for high solar activity than for low solar activity, presumably due to strong solar activity dependence of the F2-layer. No geomagnetic activity dependence was found in the F1-layer.

3.1.3. F-region peak height

The height of the F-region peak density (hmF2) occurs at the transition altitude between the chemical recombination and diffusion dominated regions, which is normally located at about 200–300 km altitude for low solar activity ($F10.7 < 120$) and 250–400 km altitude for high solar activity ($F10.7 > 120$) as can be seen in Fig. 4. This figure shows the magnetic local time variations of the hourly mean hmF2s at Millstone Hill (MH), Tromsø (EISCAT), and Svalbard (ESR) for low and high solar/magnetic activity conditions. At mid-latitude (MH), the minimum hmF2 occurs at around 08 MLT and continuously increases before it begins to decrease again at around 02 MLT and sharply drops to the minimum as the solar EUV begins to produce ions in the lower ionosphere. The diurnal variations of the mid-latitude hmF2 are broadly ranged from about 210 km altitude in winter for low solar and magnetic activities to about 410 km altitude in summer/equinox for high solar and magnetic activities. As time proceeds from day to night, the lower part of the ionosphere (E-region and F1-layer) is quickly depleted by recombination but the ionospheric plasma in the F2-layer and above is lifted upward by the equatorward neutral wind and maintained at night due to the reduced recombination at higher altitude. This wind effect sometimes results in the anomalous density structures such as the mid-latitude summer evening (or nighttime) anomaly (MSEA or MSNA) and Weddell Sea anomaly (WSA) in association with the geometry of the geomagnetic field lines (Jee et al., 2009; Klimenko et al., 2015 and references therein). The MSEA is observed at Millstone Hill in Fig. 3. As the geographic latitude increases, however, this wind effect becomes negligibly small due to the increased magnetic inclination. The maximum diurnal variation of hmF2 reaches up to about 150 km at Millstone Hill but it decreases with increasing latitude and becomes only about 30 km for solstice conditions at Svalbard for low solar and magnetic activity conditions as also reported by previous studies (Ratovsky et al., 2013, 2014). In addition to the smaller magnitude of the diurnal variations, the polar ionosphere shows fairly different phase of the

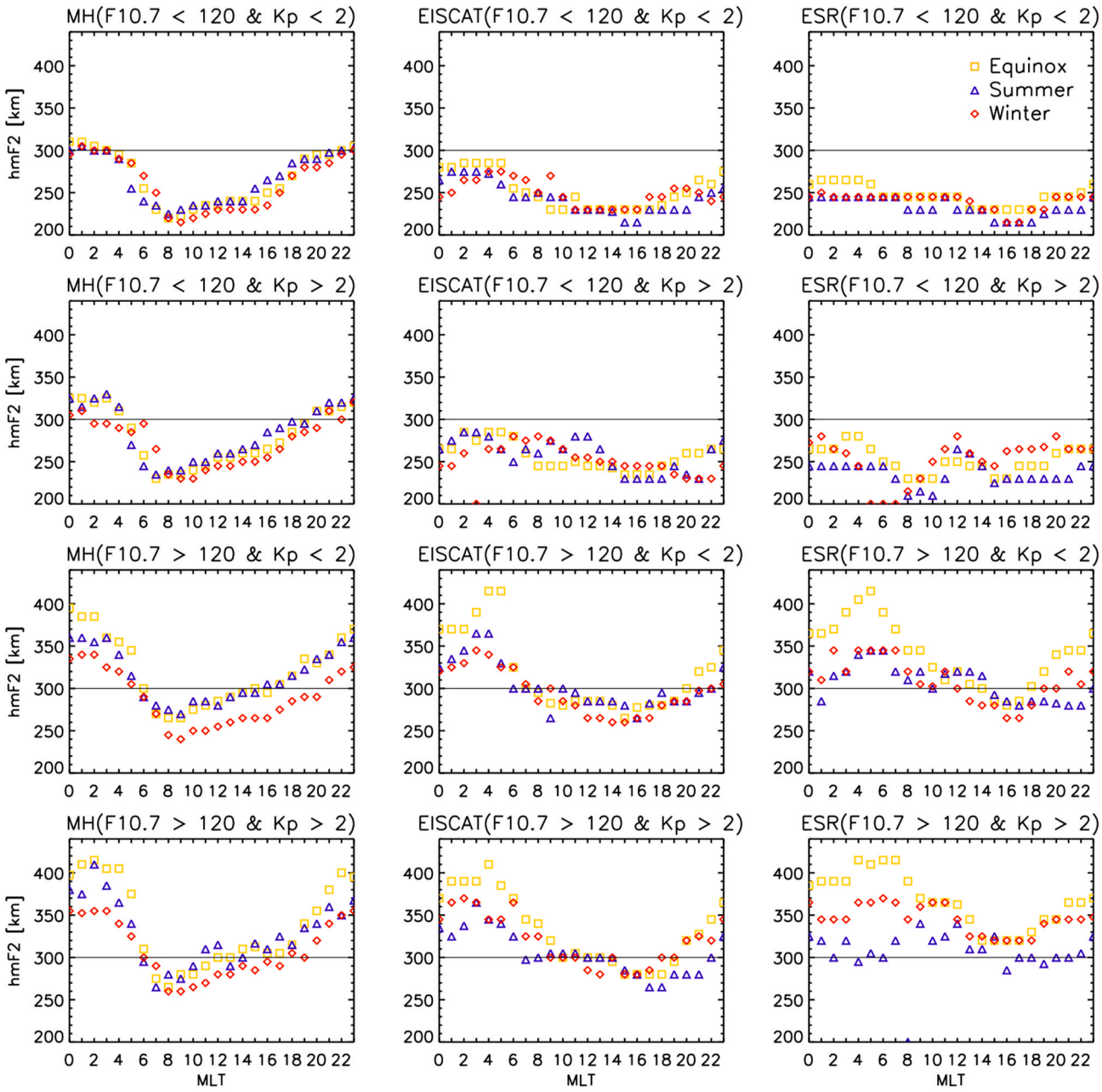

Fig. 4. Diurnal variations of hourly mean hmF2 for Equinox (yellow square), Summer (blue triangle) and Winter (red diamond) at corresponding radar stations for different F10.7 and Kp conditions as indicated in each panel.

diurnal variations of hmF2 from the mid-latitude ionosphere. The maximum and minimum hmF2s occur at around 04 MLT and 16 MLT, respectively, in the polar region while they occur at around 02 MLT and 08 MLT in the mid-latitude ionosphere.

The diurnal variations of hmF2, as well as the peak height itself, are greatly increased from low to high solar activity at all three locations. At mid-latitude, the maximum and minimum hmF2s are about 310 km and 210 km, respectively, with the diurnal variation of about 100 km for low solar activity but they are about 420 km and 250 km with the diurnal variation of about 180 km for high solar activity. Note that the variations of hmF2 with solar activity are much more significant in the polar region. For instance, the maximum and minimum hmF2s are about 290 km and 240 km, respectively, with only about 50 km diurnal variation at Tromsø in equinox for low solar activity, which is only a half of the mid-latitude, but for high solar activity they are greatly enhanced to about 420 km and 270 km with about 150-km diurnal variation, which is comparable to the mid-latitude ionosphere. It is remarkable that the hmF2 and its diurnal variations are considerably enhanced from low to high solar activity especially in the polar ionosphere. Furthermore, there are significant seasonal variations of hmF2 for high solar activity in the polar ionosphere although they are relatively small for low solar activity at all latitude regions. At Millstone Hill, hmF2 in winter is slightly smaller than the other seasons while the diurnal variations are similar for all seasons. In the polar ionosphere, hmF2 in equinox is much larger than in solstices in the early morning sector of about 00–08 MLT for high solar activity condition and this seasonal difference is particularly strong at Svalbard. It should be noted that both the diurnal and seasonal variations of the F-region density in the polar region did not show such a large enhancement with solar activity in Fig. 3. It needs to be further investigated why only the hmF2 is greatly enhanced with solar activity in the polar ionosphere.

3.1.4. Seasonal variations

We confirmed that the seasonal variations of the polar ionosphere are significant in terms of local time and height variations of the density profile in the previous section. In this section we further investigate anomalous seasonal variations such as annual, semiannual, and winter anomalies that are well known to exist in the mid-latitude ionosphere (Millward et al., 1996; Rishbeth, 1998; Rishbeth et al., 2000). There have been only a few studies on these seasonal variations in the polar ionosphere (Zhang et al., 2005; Cai et al., 2007; Xu et al., 2014). In order to investigate the seasonal variations with the extensive period of observations, we present the monthly mean density profiles of the daytime ionosphere (9–15 MLT sector) during low (left) and high (right) solar activities for quiet condition (Kp < 2) in Fig. 5. This figure clearly shows the well-known winter and semiannual anomalies at Millstone Hill for both low and high solar activity conditions and it is also true for high magnetic activity (Kp > 2). However, such seasonal variations are less evident at higher latitudes. At Tromsø (EISCAT), there seems to be semiannual anomaly for both low and high solar activity conditions, which was also noted in the four-month average densities in Fig. 3a and c. However, it is found for the first time that the semiannual anomaly at Tromsø seems to appear only for low magnetic activity (Kp < 2) but does not appear for high magnetic activity (Kp > 2). Fig. 3b and d for Kp > 2 show that the daytime F-region densities at Tromsø are largest in summer (i.e., no semiannual anomaly). The monthly mean density profiles in Fig. 5 were not presented for high magnetic activity because the data seems to be not enough to make statistically significant monthly mean density profiles for disturbed condition. No previous studies reported the semiannual anomaly in the auroral region in association with geomagnetic activity. Also note that the semiannual peaks at Tromsø appear to be shifted toward summer, compared to the peaks at Millstone Hill, which seems to be consistent with the empirical ionospheric local models developed by Zhang et al. (2005). Regarding the winter anomaly (i.e., annual anomaly in the northern hemisphere) at Tromsø, it was barely noticeable only for high solar activity and low magnetic activity condition in the very narrow (approximately 3 h) local time sector at around 14 MLT in Fig. 3c. A similar result was found at Farmer et al. (1990) and Xu et al. (2014) using the EISCAT and Dynasonde observations at Tromsø for 1981–1987 and for 1994–2005 periods, respectively. However, the daytime (09–15 MLT) mean density in Fig. 5 exhibits no winter anomaly by showing that the density in December is smaller than in June. The averaging process for 7-h daytime mean density in Fig. 5 may work to cancel the narrow density anomaly in Fig. 3c out.

At Svalbard (ESR), no semiannual anomaly exists for low solar activity but for high solar activity, it appears for both low and high magnetic activity conditions although the equinoctial peaks are a little shifted to Feb–Mar and Sep in Fig. 5. There is no sign of winter anomaly for any solar and magnetic activity conditions at Svalbard. The results of the anomalous seasonal variations are summarized in Table 2. The seasonal anomalies are usually explained by the neutral composition changes which are mainly caused by characteristic thermospheric circulations for each seasonal condition (Rishbeth et al., 2000). For instance, the summer-to-winter interhemispheric wind causes upwelling in the summer hemisphere but downwelling in the winter hemisphere,

Table 2
Anomalous seasonal variations at Millstone Hill, Tromsø, Svalbard for low and high solar activity conditions.

	Low solar activity (F10.7 < 120)	High solar activity (F10.7 > 120)
Millstone Hill **(mid-latitude)**	Semiannual anomaly Winter anomaly	Semiannual anomaly Winter anomaly
Tromsø (EISCAT) **(near auroral region)**	Semiannual (only for Kp < 2) No winter anomaly	Semiannual (only for Kp < 2) Winter anomaly (only at 12–15 MLT for Kp < 2)
Svalbard (ESR) **(near polar cap/ cusp)**	No anomaly No double-peak structure	Semiannual anomaly No winter anomaly Double-peak diurnal variation in winter

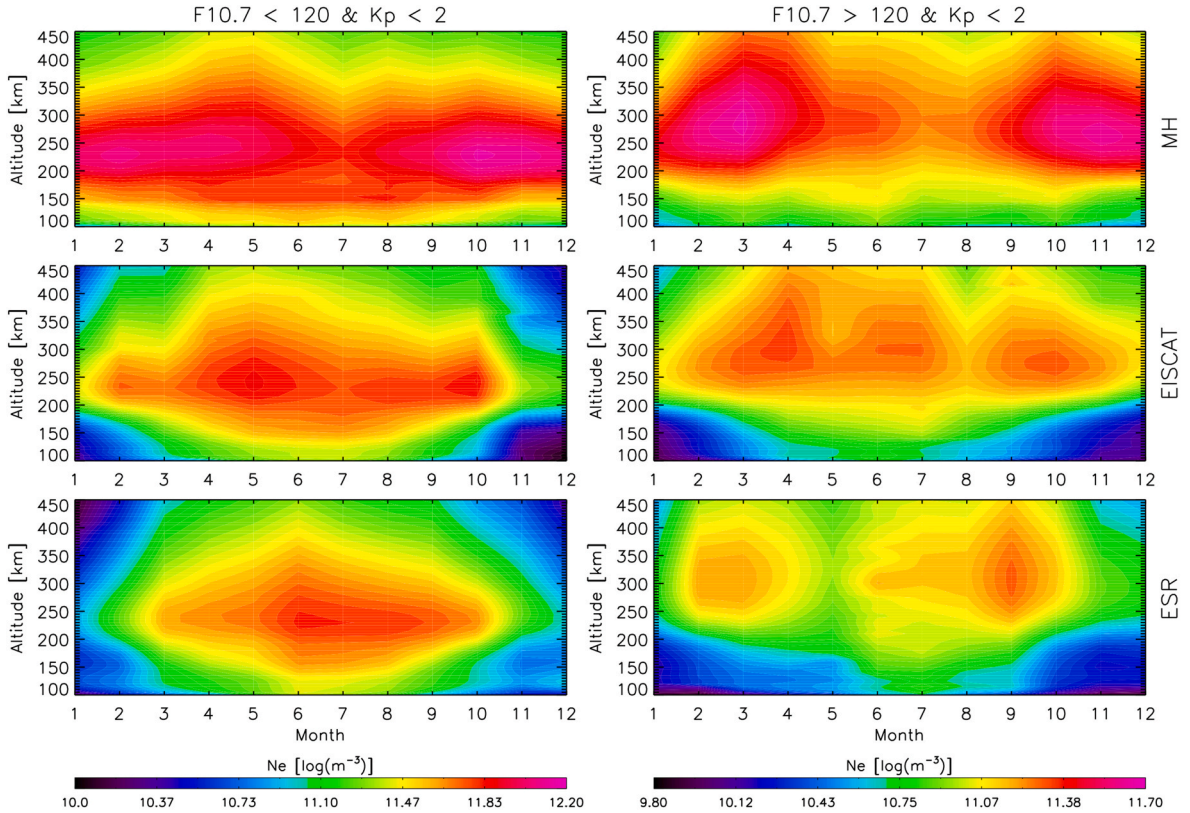

Fig. 5. Monthly mean density profiles of the daytime ionosphere (9–15 MLT) during low (left) and high (right) solar activity for geomagnetically quiet condition.

resulting in reduced and enhanced O/N_2 ratios, respectively. Furthermore, the summer-to-winter neutral wind is larger during high solar activity than during low solar activity (Hedin et al., 1994). The resulting composition changes are known to be one of the principal explanations for winter anomaly. At Tromsø and Svalbard, the NRLMSISE-00 model shows that O/N_2 ratio is largest in winter and least in summer (winter > equinox > summer) (Xu et al., 2014), which seems to be in favor of the winter anomaly even in the polar ionosphere. However, it is found that the winter anomaly hardly occurs in the polar ionosphere except for high solar and low magnetic activity condition at Tromsø as shown in Fig. 3c. In spite of being larger O/N_2 ratio in winter than in summer, a relatively weak solar production at high latitudes may not produce enough plasma to cause anomalously larger plasma density in winter as in the mid-latitude region. Furthermore, the ionospheric density is further disturbed by the magnetospheric energy inputs in the polar ionosphere such as the horizontal plasma convection, energetic particle precipitation and auroral and frictional heatings. As the solar activity increases with enhanced solar production, however, the larger O/N_2 ratio in winter seems to become effective to cause the winter anomaly even at Tromsø. As for the semiannual anomaly, Burns et al. (2012) showed that the semiannual components of NmF2 are enhanced and extended to higher latitudes with increasing solar activity, which is consistent with our results as the semiannual anomaly appears not only at Tromsø but also at Svalbard for high solar activity while it barely appears only at Tromsø but not at Svalbard for low solar activity (see Fig. 3a and c). Furthermore, it should be noted that the semiannual anomaly at Tromsø occurs only for magnetically quiet condition (Kp < 2) regardless of solar activity, which may also be related to the disturbances of the polar ionosphere by the stronger magnetospheric energy inputs during disturbed condition. In other words, this result indicates that the magnetospheric energy inputs make the unfavorable conditions for the seasonal variations in the polar ionosphere.

3.2. E-region in the polar ionosphere

The E-region ionosphere below about 150 km altitude is primarily composed of NO^+ and O_2^+ ions, and unlike the F-region ionosphere, the transports by neutral winds or electric field hardly affect the density structures due to the fast recombination in the region. The density profiles in Fig. 3 shows that, as the solar production ceases after sunset, the E-region density is quickly depleted in the mid-latitude ionosphere and also in the polar cap (Svalbard) region, except for summer when it is still sunlit even at midnight. However, we found that there are important differences between the mid-latitude and polar cap E-region ionospheres during nighttime. At mid-latitude, the nighttime E-region density profiles are severely disturbed with large irregular fluctuations below about 150 km altitude for low solar activity and the disturbed density structure is extended to higher altitude of about 200 km for high solar activity. Note that the disturbed density structure does not show any systematic altitude dependency over the entire F1- and E-region ionosphere but it is irregularly distributed with altitude. Furthermore, it does not show any dependency on the magnetic activity. The fluctuations at mid-latitude may be associated with the well-known sporadic E-layer. However, the sporadic E-layer is known to be a thin-layered enhanced density structure mostly occurring at 90–120 km altitudes, which is different from the observed structures in Fig. 3. Furthermore, the structures do not show any clear seasonal characteristics unlike summer-dominated sporadic E-layer (Mathews, 1998; Tsai et al., 2018; Yu et al., 2019). Further study seems necessary to understand the nighttime mid-latitude lower ionospheric irregularity observed at Millstone Hill. At Svalbard near the polar cap, on the other hand, the nighttime density continuously decreases with decreasing altitude all the way down the bottom of the observed profiles without showing any noticeable irregularity at least for geomagnetically quiet condition (Kp < 2). For disturbed condition (Kp > 2), there are some enhancements at the bottom of the profiles and they seem to be related to the additional ion production caused by auroral particle precipitation since the ESR location becomes closer to the auroral oval as the magnetic activity increases. This aspect will be further discussed later in this section.

In the auroral region (Tromsø), the nighttime E-region ionosphere shows a prominent density peak at about 110–120 km altitude caused by the auroral electron precipitation regardless of solar activity. The peak becomes considerably enhanced as the auroral precipitation gets stronger with increasing magnetic activity as in Fig. 3b and d. These figures also clearly show that the nighttime E-region peak density (NmE) at Tromsø is even greater than the daytime density in winter for low Kp and in all seasonal conditions for high Kp. Furthermore, the nighttime NmE is even greater than the F-region peak density for low solar activity (see Fig. 3a and b). This profile is called the E-layer dominated ionosphere (ELDI) profile (Cai et al., 2014; Mannucci et al., 2015). The ELDI is most prominent in winter for low solar activity when the solar production is minimized. It also appears in equinox for geomagnetically disturbed conditions. Note that the nighttime E-region peak height (hmE) at Tromsø slightly decreases from about 120 km to about 110 km as magnetic activity increases. This may indicate that the energy of auroral electrons on average increases with increasing magnetic activity; the electrons with higher energy penetrate deeper into the lower altitude region. According to Rees (1963), the hmE of about 110–120 km corresponds to the electron energy of about ~5 keV. Therefore, the EISCAT observations of the hmE imply that the typical energy of precipitating auroral electrons is approximately a few keV, although the auroral electrons are known to have a broad energy range from 100 eV to a few hundred keV.

The seasonal variations of the E-region density are relatively small compared to the F-region density and they seem to follow the solar zenith angle without showing anomalous behaviors in the mid-latitude ionosphere: the E-region density tends to be largest in summer but smallest in winter especially at night. In the polar ionosphere, however, the overall seasonal variations are much larger and more complicated than the mid-latitude E-region ionosphere probably due to the additional ion productions by auroral particles. In particular, it is noteworthy that the nighttime E-region density exhibits relatively small seasonal variations compared to the daytime density at Tromsø, which reveals the relative importance of the auroral precipitations to the background density without auroral precipitations. Assuming that the seasonal variations of the background E-region density basically follow the F-region density, we may be able to see the relative importance of the auroral ion production by inspecting the ratio of NmE to NmF2. Fig. 6 displays the ratios in the same format as Fig. 4. The ratios at mid-latitude exhibit the anticipated local time variations: the nighttime ratio is smaller than daytime ratio since the nighttime E-region density is negligibly small, and it is largely similar at Svalbard. The ratios at Tromsø, however, are severely deviated from the solar controlled behaviors observed in the mid-latitude and polar cap ionosphere for all conditions. First of all, the nighttime ratios are considerably larger than the daytime values, especially in winter and equinox for low solar activity. Furthermore, the nighttime ratios are enhanced at least by a factor of two from low to high magnetic activity for all seasons. This result indicates that the auroral contribution to the E-region density is extremely important during the nighttime and for high magnetic activity. Note that the nighttime NmE is greater than NmF2 (i.e., the ratio is greater than 1.0) in equinox and winter for low solar activity condition, which is the ELDI discussed earlier in this section. In summer, the ratio does not change much from day to night for low magnetic activity.

These seasonal variations suggest that the auroral contribution to the nighttime E-region density at Tromsø is largest in winter, then in equinox and smallest in summer. Does this result imply that the auroral precipitation is largest in winter and smallest in summer? A number of studies reported that the auroral electron precipitation is weaker in summer than in winter (Liou et al., 2001; Barth et al., 2004; Newell et al., 2010). Newell et al. (2010) investigated the seasonal variations of auroral precipitations using 11-year DMSP satellite data and reported

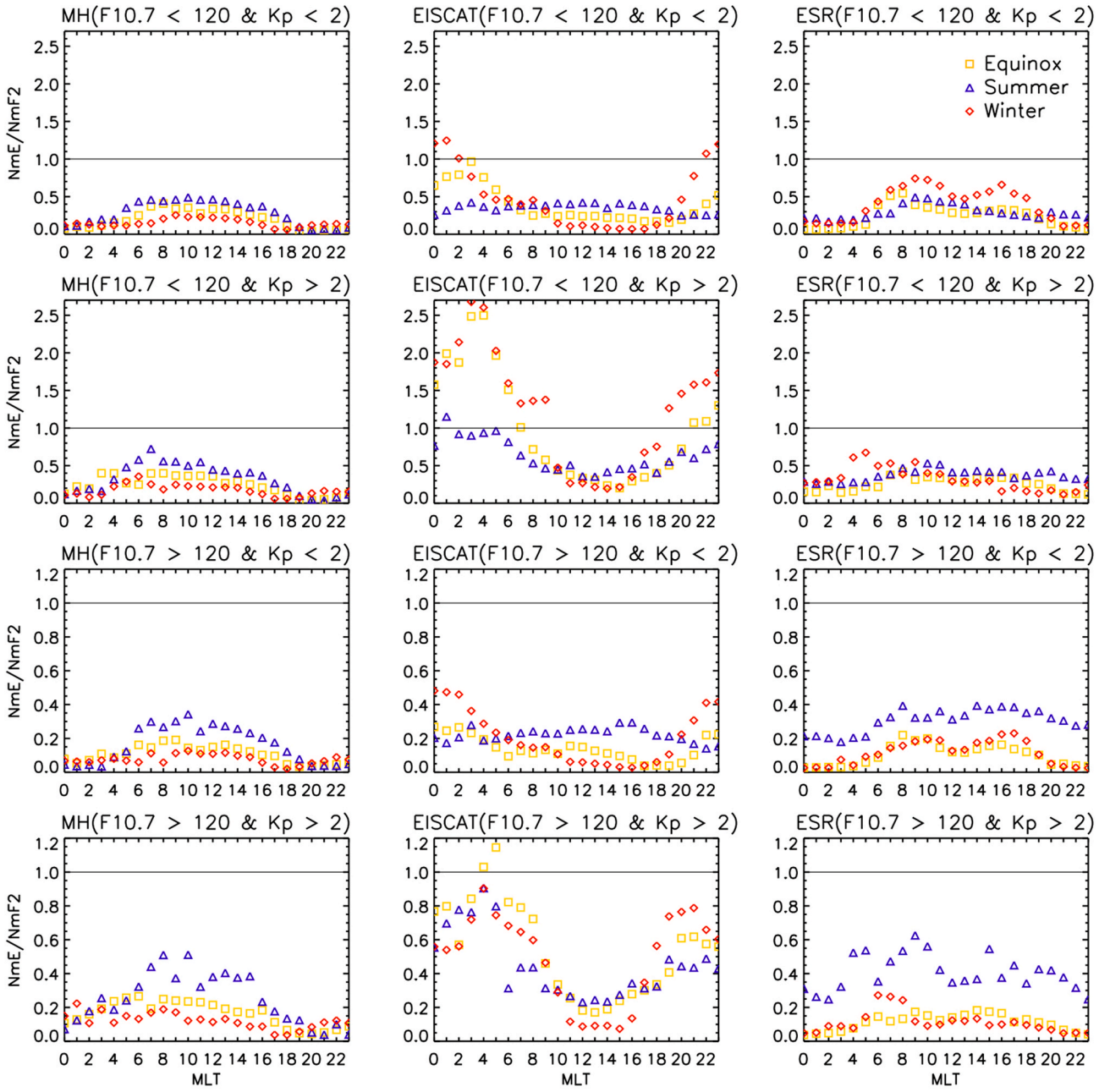

Fig. 6. Diurnal variations of the ratio of NmE to NmF2 for Equinox (yellow square), Summer (blue triangle) and Winter (red diamond) at corresponding radar stations for different F10.7 and Kp conditions as indicated in each panel.

that the nighttime auroral precipitation is generally greater in winter than in summer especially under the disturbed periods, which is consistent with the result of this study. The seasonal variation of the auroral precipitation is related to the theory that the ionospheric conductivity (i.e., ionospheric plasma density) plays a crucial role in the acceleration of auroral particles and the discrete auroral arcs are suppressed in the solar illuminated summer hemisphere. It has been reported that there is a large difference between the occurrence frequency of intense aurora in sunlight and in darkness (Newell et al., 1996, 1998, 2001; Liou et al., 2001; Barth et al., 2004; Hamrin et al., 2005). In particular, Hamrin et al. (2005) showed that the ionospheric conductivity is associated not only with intense discrete aurora but also with diffuse aurora that has been known to dominantly contribute to the magnetospheric energy input into the ionosphere (Newell et al., 2009). Furthermore, this theory may also be related to the solar activity dependence of the auroral precipitation. In Fig. 6, the seasonal variations are still present for high solar activity but to a much lesser extent: the nighttime ratios are considerably smaller than for low solar activity. This result indicates that the relative auroral contribution to the E-region density is much smaller for high solar activity than for low solar activity: The auroral precipitation does not necessarily increase with solar activity. In fact, Newell et al. (1998) argued that the occurrence frequency of intense aurora in darkness is uncorrelated with solar activity.

There are also peaks in the daytime E-region density at around 120–130 km altitude region in winter for geomagnetically quiet condition at Svalbard (Fig. 3a and c). When the solar production is small in winter at Svalbard, the energetic proton precipitation may produce a significant amount of ionization in the daytime E-region near the cusp region (Vontrat-Reberac et al., 2001). For other seasonal conditions, the

solar-EUV production may be too large to expose the proton-induced ionization in the daytime E-region. For geomagnetically disturbed condition as in Fig. 3b and d, however, the daytime E-region density peak becomes less evident, probably due to the change of the ESR location away from the cusp region.

3.3. Topside region in the polar ionosphere

In addition to the peak densities and heights of the E and F region ionosphere, the ionospheric density profiles can be further characterized by other ionospheric parameters such as topside ionospheric scale height and slab thickness. The topside ionosphere is the region above the F-region peak (hmF2) where O^+ is a dominant ion before being overtaken by H^+ ion. This region of the ionosphere is largely controlled by plasma transport processes and contains large fraction of the total electron content (TEC), which can be important for satellite communication. However, this region has been less investigated compared to the F-region and bottomside ionosphere mainly due to the limited observations. The topside ionosphere at mid-latitude is strongly coupled with the plasmasphere along the closed magnetic flux tubes, which can be very important for the maintenance of the nighttime mid-latitude ionospheric density. In the polar region, on the other hand, the topside ionosphere strongly interacts with the magnetosphere via energetic particle precipitations and ion outflows into the magnetosphere along the field lines. The different coupling processes of the ionosphere to the above regions (the plasmasphere or the magnetosphere) will result in different density structures in the topside ionosphere in the mid-latitude and polar regions.

It is immediately recognized in Fig. 3 that the density profiles of the topside ionosphere almost linearly decrease with altitude in the logarithmic density scale (i.e., exponentially decreases in the linear scale). However, the nighttime density profiles at mid-latitude show a sudden

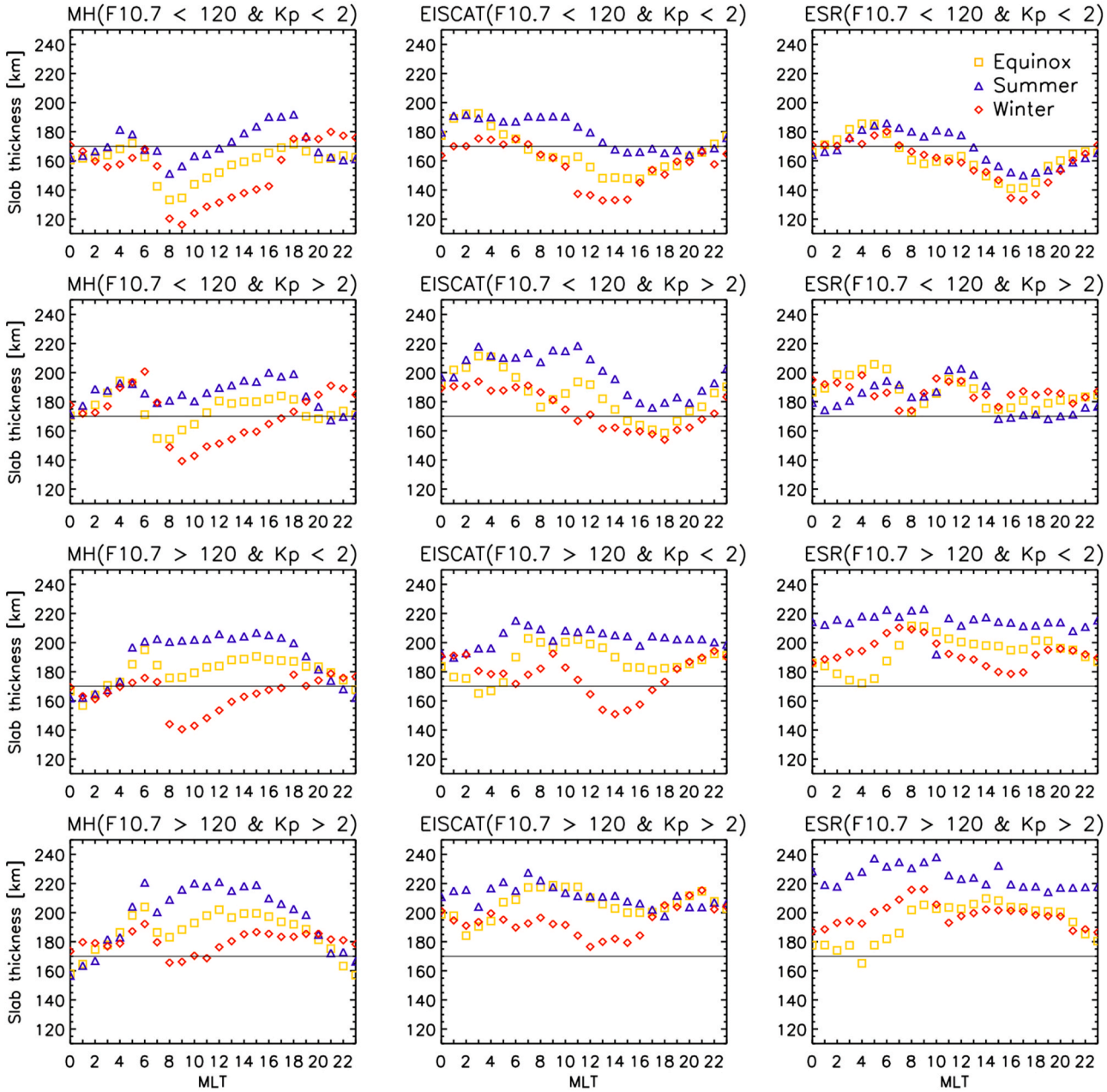

Fig. 7. Diurnal variations of hourly mean ionospheric slab thickness (IST) for Equinox (yellow square), Summer (blue triangle) and Winter (red diamond) at corresponding radar stations for different F10.7 and Kp conditions as indicated in each panel.

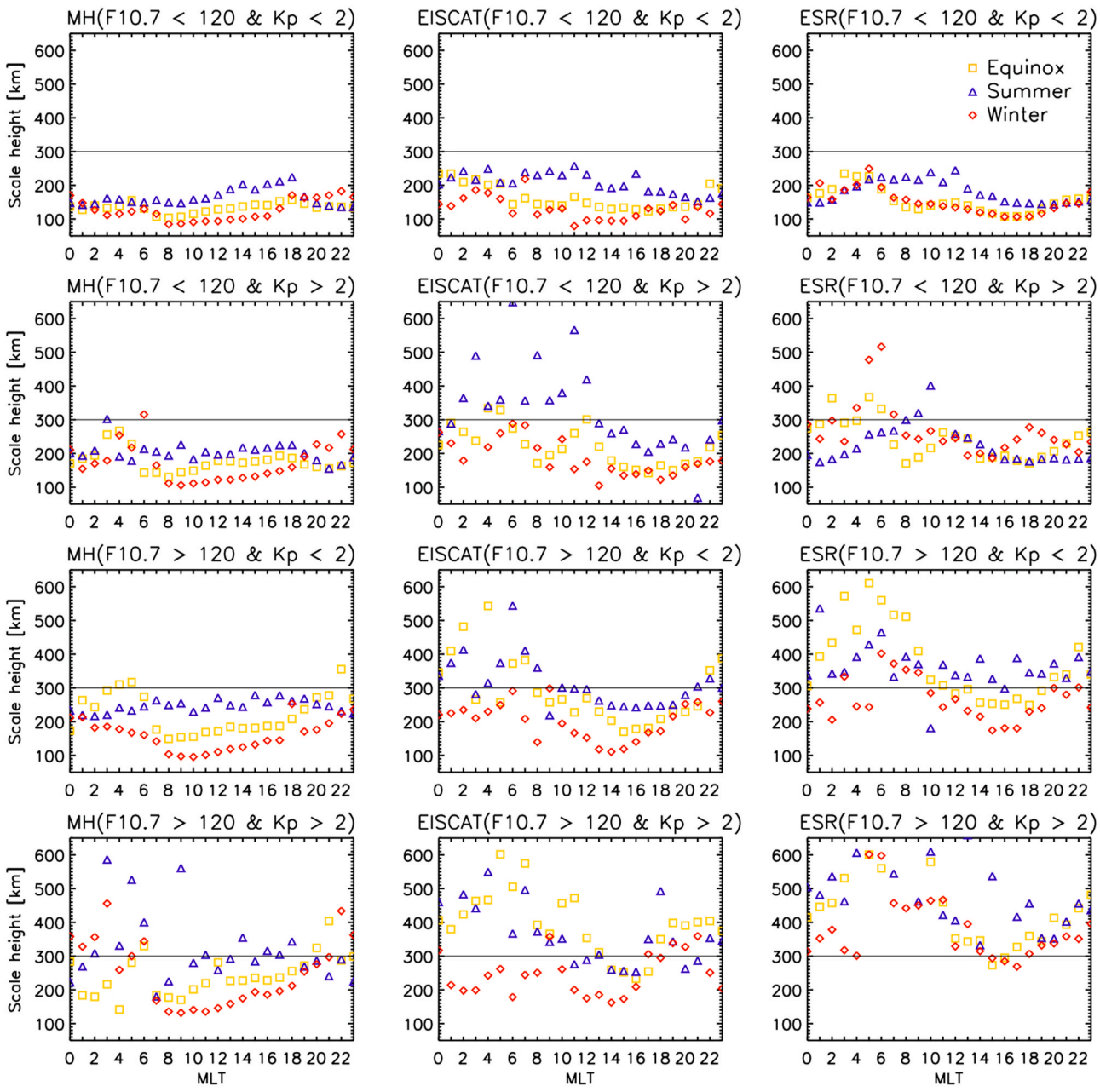

Fig. 8. Diurnal variations of hourly mean ionospheric scale height (ISH) for Equinox (yellow square), Summer (blue triangle) and Winter (red diamond) at corresponding radar stations for different F10.7 and Kp conditions as indicated in each panel.

but subtle pause at around 400 km altitude before they continue to decrease again for low solar activity. This feature seems to indicate the transition height (TH) between the ionosphere (O^+) and the plasmasphere (H^+). The transition height is lower at night than during the day, decreases from low to middle latitude and increases from low to high solar activity (Titheridge, 1976; Heelis et al., 2009; Lee et al., 2016), which explains why the transition appears only for low solar activity condition in Fig. 3 when the top boundary altitude is only 450 km for this study. This top boundary altitude is too low to show the transition height for high solar activity. As the solar activity increases, the enhanced solar EUV ionization produces the larger ionospheric density and raises the plasma temperature, which expands the whole ionosphere to higher altitude and then results in the increases of thickness around the peak and the scale height in the topside ionosphere. In order to describe the characteristics of the topside ionospheric density profiles, we calculate the ionospheric slab thickness (IST) around the F2 peak and the ionospheric scale height (ISH) above the peak, which are presented in Figs. 7 and 8, respectively in the same format as in Figs. 4 and 5.

The ionospheric slab thickness (IST) is an important parameter to describe the shape of the ionospheric density profile along with the scale height and largely determined by neutral temperature, plasma temperature and the ion composition (Titheridge, 1976; Davies and Liu, 1991; Jayachandran et al., 2004; Stankov and Warnant, 2009; Huang and Yuan, 2015). But it can also be effectively defined as the ratio of the total electron content (TEC) to the F2 peak density (i.e., IST = TEC/NmF2), which is sometimes called the equivalent slab thickness. Although the ISR measurements of the ionospheric density profile have a limited vertical range (e.g., 450 km altitude for this study due to the limited signal-to-noise ratio at higher altitude), which is much lower than the typical upper boundary of the ionosphere for TEC, it should still be meaningful to calculate the slab thickness using TEC and NmF2 from the ISR measured density profiles. Note that the ionospheric density for TEC

was integrated from 200 km to the top boundary to exclude the auroral contribution to TEC. Fig. 7 shows the calculated ISTs. At all locations, the daytime ISTs are largest in summer but smallest in winter while the nighttime ISTs show negligibly small seasonal variations. However, the IST of the polar ionosphere exhibits significant differences from the mid-latitude ionosphere in terms of both diurnal and seasonal variations. Under the low solar activity and low magnetic activity condition (top panels in Fig. 7), the minimum IST of the mid-latitude ionosphere occurs just after the sunrise and it continues to increase until around the sunset for all season but the deepest minimum occurs in winter. These diurnal variations little change even for high magnetic activity except that the thickness seems to be slightly enhanced. For high solar activity, the daytime ISTs are substantially changed while the nighttime values show little changes. The daytime ISTs are significantly enhanced for all seasonal conditions and become larger than nighttime values in equinox and summer. This solar activity dependence of the mid-latitude IST is consistent with Jayachandran et al. (2004). The diurnal variation of the polar IST is nearly opposite to the mid-latitude ionosphere: the large IST around the sunrise continuously decreases until the around the sunset and then rises again. The diurnal variations in general become weaker for high solar activity than for low solar activity but it is hard to find any systematic diurnal variations for high solar activity. Jayachandran et al. (2004) reported that the nighttime IST is larger than the daytime IST for both solar minimum and maximum periods in the auroral region. But our results do not show such a tendency in the polar region except for winter at Tromsø. It is important to note that the IST tends to increase with increasing latitude for high solar activity, particularly in summer, but there is no such a tendency with latitude for low solar activity. Furthermore, the IST tends to increase with increasing solar activity particularly at Svalbard. This difference implies that the slab thickness more strongly responds to solar activity in the polar ionosphere (Jayachandran et al., 2004; Stankov and Warnant, 2009 and references therein). Also noted is that the seasonal variabilities are significantly enhanced for high solar activity. With regard to the variations with magnetic activity, the overall ISTs are slightly enhanced from low to high magnetic activity for both solar activity conditions.

The ionospheric scale height (ISH) is often used to characterize the ionospheric density profile especially in the topside ionosphere. It is a critical parameter in the modeling efforts to reconstruct the topside ionospheric density profiles from the ionospheric radio occultation technique (e.g., Hajj and Romans, 1998) or ground-based ionospheric sounding and GPS TEC measurements (Stankov et al., 2003) and also in the empirical models such as the International Reference Ionosphere (IRI) (e.g., Ram et al., 2009). Under the diffusive equilibrium condition, the density in the topside ionosphere decreases exponentially with altitude at a rate governed by the plasma scale height. It describes the relationship between ionospheric density, temperature and relative ion concentration (Watt, 1965) and defined by either $-\ dh/\ d(\ln(N_e))$ or kT_p/mg (Rishbeth and Garriott, 1969). In this study, we calculated the topside scale height using the first definition from the hourly-mean density profiles shown in Fig. 3. The linear fitting was applied to the density profiles between the top boundary and 30 km altitude above the hmF2 to calculate density gradient. This procedure was discussed in detail at Kutiev et al. (2006). Fig. 8 shows the calculated ISHs. The differences in the overall magnitude and diurnal variations of ISH between the mid-latitude and the polar ionosphere are relatively small for low solar activity, but they are noticeably enhanced for high solar activity. Although the mid-latitude ISHs are only slightly increased from low to high solar activity, the ISHs in the polar region are greatly increased especially in the morning sector (00–08 MLT). The largest increase occurs at Svalbard: the ISHs in the early morning (02–06 MLT) are increased from about 200 km for low solar activity to about 600 km for high solar activity in equinox. Note that similar change of diurnal variations with solar activity was also found at the hmF2 in the polar region: the increase of ISHs in the morning sector may be related to the elevated height for the determination of ISH. With regard to the variations of ISH with magnetic activity, only the nighttime ISHs are enhanced for high Kp at mid-latitude. In the polar region, however, the ISH seems to be generally enhanced with magnetic activity, particularly at Svalbard for high solar activity. It is noticeable that the diurnal variations are scattered with large variations for high solar and magnetic activity condition regardless of season and latitude. This large scatter may result from the statistical problems of the data for high solar and magnetic activity condition, but it didn't occur for hmF2 and IST although they are obtained from the same hourly-mean density profiles. Therefore, the large scatter of ISH may indicate the large disturbances of the topside density profiles for high magnetic activity. Liu et al. (2007) also reported that the variability of ISH is enhanced under disturbed conditions at Millstone Hill.

As for the seasonal variations, the daytime ISHs are clearly largest in summer but smallest in winter at mid-latitude, which is consistent with Liu et al. (2007). Around the midnight, however, the seasonal variations of the mid-latitude ISH are negligibly small or slightly larger in winter than in summer, which agrees with Stankov and Jakowski (2006). Overall, these seasonal characteristics are still true at Tromsø but becomes less evident at Svalbard, particularly for high magnetic activity at which no systematic seasonal variations are found. As mentioned earlier, the fundamental differences between the mid-latitude and polar topside ionospheres may come from the fact that the topside ionosphere in the polar region is directly coupled to the magnetosphere while the mid-latitude ionosphere is coupled to the plasmasphere. Aside from the electromagnetic coupling to the magnetosphere in the polar region, the exchanges of ions between the topside ionosphere and the magnetosphere via ion upflow/outflow must be responsible for the differences from the mid-latitude ionosphere which exchanges ions with the plasmasphere. Further study is necessary to understand how these coupling processes in the topside ionosphere produce the differences between the mid-latitude and polar ionosphere.

4. Summary and conclusion

Using long-term ISR observations for the period of 1995–2015, we investigated the climatological characteristics of the entire electron density profiles in the polar region at Tromsø and Svalbard (66°N and 75°N MLAT, respectively), in comparison with the density profiles in the mid-latitude ionosphere at Millstone Hill (53°N MLAT). The analysis was performed on the density variations with local time, season, solar and magnetic activities. We summarize the results as follows.

1. In the polar ionosphere, the diurnal variations of the F-region density profiles are much smaller than in the mid-latitude ionosphere and in particular, it is extremely small in summer. In winter, however, when the solar EUV radiation is almost absent, other ion productions and transport processes become more effective to produce characteristic features of the polar ionosphere such as the double-peak structure occurring at Svalbard during high solar activity.
2. The diurnal variations of hmF2 are clearly reduced in the polar region especially for low solar activity but they become comparable to the mid-latitude ionosphere for high solar activity: hmF2 and its diurnal variations are remarkably enhanced from low to high solar activity in the polar ionosphere. The minimum and maximum hmF2s occur at 16–18 MLT and 04–06 MLT sectors, respectively in the polar region while they occur at around 08 MLT and just after the midnight at mid-latitude. The seasonal variations of hmF2 are mostly small for low solar activity but become fairly large at Svalbard (especially in equinox) for high solar activity.
3. The well-known semiannual and winter anomalies generally occurring in the mid-latitude ionosphere are less evident in the polar ionosphere. At Tromsø, the semiannual anomaly occurs only for low magnetic activity and the winter anomaly exists at

very narrow local time sector of 12–15 MLT only for high solar activity and low magnetic activity condition. At Svalbard, no anomaly occurs except for the semiannual anomaly occurring only for high solar activity. It seems that the magnetospheric energy inputs make the unfavorable conditions for the seasonal variations in the polar ionosphere.

4. The mid-latitude F1-layer becomes less distinctive in winter than in summer and also for high solar activity than for low solar activity. No dependence of geomagnetic activity was found in the F1-layer. However, the F1-layer nearly disappears in the polar region, especially at Svalbard
5. As expected from the existence of the auroral precipitation, the nighttime E-region ionosphere at Tromsø is distinguished from Millstone Hill and Svalbard by characteristic density peaks at around 110–120 km altitude. The E-region density peaks (NmEs) are considerably enhanced for high magnetic activity, even being larger than NmF2 in winter for low solar activity (i.e., ELDI).
6. The mid-latitude nighttime E-region ionosphere shows severe small-scale irregular fluctuations regardless of season and solar and magnetic activities, but no such fluctuations exist in the polar region.
7. The variations of NmE/NmF2 ratio representing the auroral contribution to the E-region density indicate that the auroral precipitation is largest in winter and smallest in summer. Furthermore, the relative auroral contribution to the E-region density is much smaller for high solar activity than for low solar activity, which may imply that the auroral precipitation does not necessarily increase with solar activity.
8. At Svalbard, the energetic proton precipitation causes the daytime E-region density peak at around 125 km altitude in winter for low magnetic activity when the ESR locates near the cusp region but it becomes less evident for high magnetic activity probably due to the change of the ESR location away from the cusp region.
9. Under the low solar activity and low magnetic activity condition, the minimum IST of the mid-latitude ionosphere occurs just after the sunrise and it continues to increase until around the sunset for all seasons. However, the polar ionosphere shows nearly opposite diurnal variation. The IST tends to increase from the mid-latitude to high latitudes for high solar activity, especially in summer being largest at Svalbard. The magnetic activity effect appears to be relatively small. The overall magnitude of IST is largest in summer but smallest in winter.
10. The ISH shows relatively small differences between the mid-latitude and the polar region for low solar activity, but the ISH is generally enhanced with increasing latitude for high solar activity. Furthermore, the diurnal variations of ISH in the polar region are more substantially enhanced from low to high solar activity with maximum in the early morning (02–06 MLT) and minimum in the afternoon (14–18 MLT). The ISH shows a large scatter for high magnetic activity, which may indicate the large disturbances of the topside density profiles.

As a concluding remark, it is found that the ionospheric density profiles in the polar region show much more complicate variabilities with local time, season, and solar and magnetic activities, compared to the mid-latitude ionosphere. Furthermore, the polar ionosphere generally responds to increasing solar and magnetic activities in a stronger and more complex way than the mid-latitude ionosphere probably due to the magnetospheric energy inputs. In order to investigate these variabilities of the polar ionospheric density profiles, more extensive and continuous observations are necessary since the current observations from the ground and space are far from being adequate to reveal the complete variabilities of the polar ionosphere. Among the ongoing efforts to enhance the observations for the polar ionosphere, the EISCAT scientific association is preparing for a next generation radar system called EISCAT 3D to greatly strengthen the existing observation capability for the Earth's atmosphere and ionosphere in the Arctic. The EISCAT 3D will measure the spectra of radio-waves that are backscattered from free electrons that are controlled by inherent ion-acoustic and electron plasma waves in the ionosphere, which will reveal high-resolution information on the ionospheric plasma parameters. Unlike the current EISCAT radars, the new ISR will have the capability of producing volumetric images of ionospheric parameters in the extended spatial area with simultaneous full-vector drift velocities (Stamm et al., 2020; https://www.eiscat.se/eiscat3d-information/). In Antarctica, Korea Polar Research Institute (KOPRI) has been started monitoring the polar ionosphere as well as the thermosphere and magnetosphere using various ground instruments such as Vertical Incidence Pulsed Ionospheric Radar (VIPIR)/Dynasonde, GPS TEC/Scintillation monitor, Fabry-Perrot Interferometer (FPI), magnetometers, and auroral All Sky Camera at Jang Bogo Station (JBS), Antarctica (Kwon et al., 2018; Ham et al., 2020). These new observations will be greatly beneficial to the space science community to further investigate and understand the complex variabilities of the polar ionospheric density.

Declaration of competing interest

The authors declare that they have no known competing financial interests or personal relationships that could have appeared to influence the work reported in this paper.

Acknowledgements

This work was supported by research grant PE20100 from Korea Polar Research Institute (KOPRI). Y.-S. Kwak was supported by basic research funding from Korea Astronomy and Space Science Institute (KASI) and by Air Force Office of Scientific Research (AFOSR)/Asian Office of Aerospace Research and Development (AOARD) grant FA2386-18-1-0107. The EISCAT and ESR data are obtained from NIPR database (pc115.seg20.nipr.ac.jp/www/eiscatdata/ne_te_ti_vi.html) and Millstone Hill ISR data is downloaded from Madrigal CEDAR database (http://cedar.openmadrigal.org). The EISCAT is an international association supported by research organizations in China (CRIRP), Finland (SA), Japan (NIPR and ISEE), Norway (NFR), Sweden (VR), and the United Kingdom (UKRI). KOPRI and KASI have been participating EISCAT as Affiliates since 2015.

References

Baron, M.J., 1974. Electron densities within aurorae and other auroral E-region characteristics. Radio Sci. 9 (2), 341–348.

Barth, C.A., Baker, D.N., Bailey, S.M., 2004. Seasonal variation of auroral electron precipitation. Geophys. Res. Lett. 31, L04809. https://doi.org/10.1029/2003GL018892.

Burns, A.G., Solomon, S.C., Wang, W., Qian, L., Zhang, Y., Paxton, L.J., 2012. Daytime climatology of ionospheric NmF2 and hmF2 from COSMIC data. J. Geophys. Res. 117, A09315.

Cai, H.T., Ma, S.Y., Fan, Y., Liu, Y.C., Schlegel, K., 2007. Climatological features of electron density in the polar ionosphere from long-term observations of EISCAT/ESR radar. Ann. Geophys. 25, 2561–2569.

Cai, H.T., Li, F., Shen, G., Zhan, W., Zhou, K., McCrea, I.W., Ma, S., 2014. E layer dominated ionosphere observed by EISCAT/ESR radars during solar minimum. Ann. Geophys. 32, 1223–1231.

Caton, R., Horwitz, J.L., Richards, P.G., Liu, C., 1996. Modeling of F-region ionospheric upflows observed by EISCAT. Geophys. Res. Lett. 23 (12), 1537–1540. https://doi.org/10.1029/96gl01255.

Dandekar, B.S., 2002. Solar cycle dependence of polar cap patch activity. Radio Sci. 37 (1), 1013.

Davies, K., Liu, X.M., 1991. Ionospheric slab thickness in middle and low latitudes. Radio Sci. 26 (4), 997–1005.

Farmer, A.D., Crothers, S.R., Davda, V.N., 1990. The winter anomaly at Tromsø. J. Atmos. Terr. Phys. 52 (6–8), 561–568.

Fontaine, D., 2002. Structure and dynamics of the Earth's polar ionosphere: recent results inferred from incoherent scatter sounders. Plasma Sources Sci. Technol. 11, A113–A119.

Forster, M., Haaland, S., 2015. Interhemispheric differences in ionospheric convection: cluster EDI observations revisited. J. Geophys. Res. 120, 5805–5823.

Gonzalez, W.D., Gonzalez, A.L.C., Tsurutani, B.T., 1990. Dual-peak solar cycle distribution of intense geomagnetic storms, planet. Space Sci 38 (2), 181–187.
Hajj, G.A., Romans, L.J., 1998. Ionospheric electron density profiles obtained with the GPS: results from GPS/MET experiment. Radio Sci. 33, 175–190.
Ham, Y., Jee, G., Lee, C., Kwon, H.-J., Kim, J.-H., 2020. Observations of the polar ionosphere by the vertical incidence pulsed ionospheric radar at Jang Bogo station, Antarctica. Journal of Astronomy and Space Sciences 37 (2), 143–156. https://doi.org/10.5140/JASS.2020.37.2.143.
Hamrin, M., Norqvist, P., Rönnmark, K., Fellgård, D., 2005. The importance of solar illumination for discrete and diffuse aurora. Ann. Geophys. 23, 3481–3486.
Hargreaves, J.K., Ranta, H., Ranta, A., Turunen, E., Turunen, T., 1987. Observations of the polar cap absorption event of February 1984 by the EISCAT incoherent scatter radar, Planet. Space Sci 35 (7), 947–958.
Hedin, A.E., Buonsanto, M.J., Codrescu, M., Duboin, M.L., Fesen, C.G., Hagan, M.E., Miller, K.L., Sipler, D.P., 1994. Solar activity variations in midlatitude thermospheric meridional winds. J. Geophys. Res. 99 (A9), 17601–17608.
Heelis, R.A., Coley, W.R., Burrell, A.G., Hairston, M.R., Earle, G.D., Perdue, M.D., Power, R.A., Harmon, L.L., Holt, B.J., Lippincott, C.R., 2009. Behavior of the O+/H+ transition height during the extreme solar minimum of 2008. Geophys. Res. Lett. 36, L00C03, 10.1029/2009GL038652.
Huang, Z., Yuan, H., 2015. Climatology of the ionospheric slab thickness along the longitude of 120E in China and its adjacent region during the solar minimum years of 2007-2009. Ann. Geophys. 33, 1311–1319, 10.594/angeo-33-1311-2015.
Hunsucker, R.D., 1975. Chatanika radar investigation of high latitude E-region ionization structure and dynamics. Radio Sci. 10 (3), 277–288.
Jayachandran, B., Krishnankutty, T.N., Gulyaeva, T.L., 2004. Climatology of ionospheric slab thickness. Ann. Geophys. 22, 25–33.
Jee, G., Burns, A.G., Kim, Y.H., Wang, W., 2009. Seasonal and solar activity variations of the Weddell Sea Anomaly observed in the TOPEX total electron content measurements. Journal of Geophysical Research - Atmosphere 114 (A4), A04307. https://doi.org/10.1029/2008ja013801.
Klimenko, M.V., Klimenko, V.V., Karpachev, A.T., Ratovsky, K.G., Stepanov, A.E., 2015. Spatial features of Weddell Sea and Yakutsk Anomalies in foF2 diurnal variations during high solar activity periods: interkosmos-19 satellite and ground-based ionosonde observations, IRI reproduction and GSM TIP model simulation. Adv. Space Res. 55, 2020–2032.
Kutiev, I.S., Marinov, P.G., Watanabe, S., 2006. Model of topside ionosphere scale height based on topside sounder data. Adv. Space Res. 37, 943–950. https://doi.org/10.1016/j.asr.2005.11.021.
Kwon, H.-J., Lee, C., Jee, G., Ham, Y., Kim, J.-H., Kim, Y.H., Kim, K.-H., Wu, Q., Bullett, T., Oh, S., Kwak, Y.-S., 2018. Ground-based observations of the polar region space environment at the Jang Bogo station, Antarctica. Journal of Astronomy and Space Sciences 35 (3), 185–193. https://doi.org/10.5140/jass.2018.35.3.185.
Le, G.-M., Cai, Z.-Y., Wang, H.-N., Yin, Z.-Q., Li, P., 2013. Solar cycle distribution of major geomagnetic storms. Res. Astron. Astrophys. 13 (6), 739–748.
Lee, H.-B., Kim, Y.H., Kim, E., Hong, J., Kwak, Y.-S., 2016. Where does the plasmasphere begin? Revisit to topside ionospheric profiles in comparison with plasmaspheric TEC from Jason-1. J. Geophys. Res. 121, 10091–10102.
Liou, K., Newell, P.T., Meng, C.-I., 2001. Seasonal effects on auroral particle acceleration and precipitation. J. Geophys. Res. 106 (A4), 5531–5542.
Liu, L., Wan, W., Zhang, M.-L., Ning, B., Zhang, S.-R., Holt, J.M., 2007. Variations of topside ionospheric scale heights over Millstone Hill during the 30-day incoherent scatter radar experiment. Ann. Geophys. 25, 2019–2027.
Mannucci, A.J., Tsurutani, B.T., Verkhoglyadova, O., Komjathy, A., Pi, X., 2015. Use of radio occultation to probe the high-latitude ionosphere. Atmos. Measurement Techniques 8, 2789–2800.
Mathews, J.D., 1998. Sporadic E: current views and recent progress. J. Atmos. Sol. Terr. Phys. 60 (4), 413–435.
Millward, G.H., Rishbeth, H., Fuller-Rowell, T.J., Aylward, A.D., Quegan, S., Moffett, R. J., 1996. Ionospheric F2 layer seasonal and semiannual variations. J. Geophys. Res. 101 (A3), 5149–5156.
Moen, J., Qiu, X.C., Carlson, H.C., Fujii, R., McCrea, I.W., 2008. On the diurnal variability in F2-region plasma density above the EISCAT Svalbard radar. Ann. Geophys. 26, 2427–2433.
Newell, P.T., Meng, C.-I., Lyons, K.M., 1996. Discrete aurorae are suppressed in sunlight. Nature 381, 766.
Newell, P.T., Meng, C.-I., Wing, S., 1998. Relation to solar activity of intense aurorae in sunlight and darkness. Nature 393, 342.
Newell, P.T., Greenwald, R.A., Ruohoniemi, J.M., 2001. The role of the ionosphere in aurora and space weather. Rev. Geophys. 39, 137. https://doi.org/10.1029/1999RG000077.
Newell, P.T., Sotirelis, T., Wing, S., 2009. Diffuse, monoenergetic, and broadband aurora: the global precipitation budget. J. Geophys. Res. 114, A09207. https://doi.org/10.1029/2009JA014326.
Newell, P.T., Sotirelis, T., Wing, S., 2010. Seasonal variations in diffuse, monoenergetic, and broadband aurora. J. Geophys. Res. 115, A03216. https://doi.org/10.1029/2009JA014805.
Obridko, V.N., Kanonidi, Kh D., Mitrofanova, T.A., Shelting, B.D., 2013. Solar activity and geomagnetic disturbances. Geomagn. Aeron. 53 (2), 147–156.
Ranta, A., Ranta, H., Turunen, T., Silen, J.J., Stauning, P., 1985. High resolution observations of D-region by EISCAT and their comparison to riometer measurements, Planet. Space Sci 33 (6), 583–589.
Ram, T.S., Su, S.-Y., Liu, C.H., Reinisch, B.W., McKinnell, L.-A., 2009. Topside ionospheric effective scale heights (HT) derived with ROCSAT-1 and ground-based ionosonde observations at equatorial and midlatitude stations. J. Geophys. Res. 114, A10309. https://doi.org/10.1029/2009JA014485.f.
Ratovsky, K.G., Oinats, A.V., Medvedev, A.V., 2013. Regular features of the polar ionosphere characteristics from Digisonde measurements over Norilsk. Adv. Space Res. 51, 545–553.
Ratovsky, K.G., Shi, J.K., Oinats, A.V., Raomanova, E.B., 2014. Comparative study of high-latitude, mid-latitude and low-latitude ionosphere on basis of local empirical models. Adv. Space Res. 54, 509–516.
Rees, M.H., 1963. Auroral ionization and excitation by incident energetic electrons. Planet. Space Sci. 11, 1209–1218.
Rishbeth, H., Garriott, O.K., 1969. Introduction to Ionospheric Physics, first ed. Academic Press, New York, pp. 87–125 (Chapter 3).
Rishbeth, H., Van Eyken, A.P., 1993. EISCAT: early history and the first ten years of operation. J. Atmos. Terr. Phys. 55, 525–542.
Rishbeth, H., 1998. How the thermospheric circulation affects the ionospheric F2-layer. J. Atmos. Sol. Terr. Phys. 60, 1385–1402.
Rishbeth, H., Muller-Wodarg, I.C.F., Zou, L., Fuller-Rowell, T.J., Millward, G.H., Moffett, R.J., Idenden, D.W., Aylward, A.D., 2000. Annual and semiannual variations in the ionospheric F2-layer: II. Physical discussion. Ann. Geophys. 18, 945–956.
Stamm, J., Vierinen, J., Urco, J.M., Gustavsson, B., Chau, J.L., 2020. Radar imaging with EISCAT 3D. Ann. Geophys. https://doi.org/10.5194/angeo-2020-28.
Stankov, S.M., Jakowski, N., Heise, S., Muhtarov, P., Kutiev, I., Warnant, R., 2003. A new method for reconstruction of the vertical electron density distribution in the upper ionosphere and plasmasphere. J. Geophys. Res. 108 (A5), 1164. https://doi.org/10.1029/2002JA009570.
Stankov, S.M., Jakowski, N., 2006. Topside ionospheric scale height analysis and modeling based on radio occultation measurements. J. Atmos. Sol. Terr. Phys. 68, 134–162.
Stankov, S.M., Warnant, R., 2009. Ionospheric slab thickness—analysis, modelling and monitoring. Adv. Space Res. 44 (11), 1295–1303. https://doi.org/10.1016/j.asr.2009.07.010.
Titheridge, J.E., 1976. Ion transition heights from topside electron density profiles, Planet. Space Sci 24, 229–246, 10.1016/0032- 0633(76)90020-9.
Tsai, L.-C., Su, S.-Y., Liu, C.-H., Schuh, H., Wickert, J., Alizadeh, M.M., 2018. Global morphology of ionospheric sporadic E layer from the FormoSat-3/COSMIC GPS radio occultation experiment. GPS Sol 22, 118.
Vallinkoski, M., Lehtinen, M.S., 1990. The effect of a priori knowledge on parameter estimation errors with applications to incoherent scatter. J. Atmos. Terr. Phys. 52 (6–8), 675–685.
Vontrat-Reberac, A., Fontaine, D., Blelly, P.-L., Galand, M., 2001. Theoretical predictions of the effect of cusp and dayside precipitation on the polar ionosphere. J. Geophys. Res. 106 (A12), 28857–28865.
Watt, T.M., 1965. Ion distribution and temperature in the topside ionosphere obtained from the Alouette Satellite. J. Geophys. Res. 70 (23).
Xiong, C., Luhr, H., Wang, H., Johnsen, M.G., 2014. Determining the boundaries of the auroral oval from CHAMP field-aligned current signatures – Part 1. Ann. Geophys. 32, 609–622.
Xu, S., Zhang, B., Liu, R., Guo, L., Wu, Y., 2014. Comparative studies on ionospheric climatological features of NmF2 among the Arctic and Antarctic stations. J. Atmos. Sol. Terr. Phys. 119, 63–70.
Yu, B., Xue, X., Yue, X., Yang, C., Yu, C., Dou, X., Ning, B., Hu, L., 2019. The global climatology of the intensity of the ionospheric sporadic E layer. Atmos. Chem. Phys. 19, 4139–4145.
Zhang, S.R., Holt, J.M., van Eyken, A.P., McCready, M., Amory-Mazaudier, C., Fukao, S., Sulzer, M., 2005. Ionospheric local model and climatology from long-term databases of multiple incoherent scatter radars. Geophys. Res. Lett. 32, L20102.